



Passivated *n–p* co-doping of niobium and nitrogen into self-organized TiO_2 nanotube arrays for enhanced visible light photocatalytic performance

Zhengchao Xu^a, Weiyi Yang^a, Qi Li^{a,*}, Shian Gao^a, Jian Ku Shang^{a,b}

^a Environment Functional Materials Division, Shenyang National Laboratory for Materials Science, Institute of Metal Research, Chinese Academy of Sciences, Shenyang, 110016, PR China

^b Department of Materials Science and Engineering, University of Illinois at Urbana-Champaign, Urbana, IL 61801, USA



ARTICLE INFO

Article history:

Received 4 May 2013

Received in revised form 7 July 2013

Accepted 15 July 2013

Available online 24 July 2013

Keywords:

Passivated *n–p* co-doping

Niobium

Nitrogen

TiO_2 nanotube arrays

Enhanced visible light photocatalytic performance

ABSTRACT

Passivated *n–p* co-doping of niobium and nitrogen was successfully incorporated into self-organized TiO_2 nanotube arrays by anodizing Ti–Nb alloys, followed with the heat treatment in a flow of ammonia gas. Nb was doped into TiO_2 nanotube arrays during the anodization by substituting Ti^{4+} with Nb^{5+} , while N was doped into TiO_2 nanotube arrays during the heat treatment by substituting O^{2-} with N^{3-} . Since Nb in TiO_2 enhanced the adsorption of NH_3 molecules onto the nanotube arrays, Nb doping was found to promote the subsequent N doping into the anatase lattice. As predicted by first-principles band structure calculations, Nb/N co-doped titanium oxide nanotube arrays demonstrated a largely enhanced visible light response and visible light photocatalytic performance on the degradation of methylene blue, compared to TiO_2 nanotube arrays or TiO_2 nanotube arrays with either dopant. The passivated *n–p* co-doping approach may also be applied to other material systems and promise a wide range of technical applications.

© 2013 Elsevier B.V. All rights reserved.

1. Introduction

Highly ordered TiO_2 nanotube arrays made by anodization of titanium in fluoride-based electrolyte solutions have attracted a lot of research interest in recent years due to the unique properties from this particular TiO_2 architecture [1–11]. Because of their large surface area, more efficient absorption of incident photons, and decreased bulk recombination, highly ordered TiO_2 nanotube arrays possessed enhanced photocatalytic and photoelectrochemical properties [7,8]. Furthermore, nanotube arrays could have relatively higher crystal lattice distortion, leading to lower band-to-band transition energy and subsequently better visible light absorption [7].

Doping could change the material structure and introduce novel properties that un-doped materials could not have [12–14]. Since the pioneering work of Asahi et al. [15], doping of nonmetal anionic elements, especially nitrogen, has been explored extensively to improve the visible light absorption of TiO_2 due to the modification of its band structure by creating an acceptor level above the valence band maximum (VBM) [15–18]. However, it is well known

that the massive charge carrier recombination caused by nitrogen-doping could largely limit the photoactivity of nitrogen-doped TiO_2 [16,19]. Another doping strategy of transition-metal doping has also been examined extensively, which could expand the light absorption of TiO_2 into the visible light region [20–22]. However, the existence of charge carrier recombination centers and strongly localized *d* states within the band gap largely limit the charge carrier mobility [23–25]. Although various transition-metal/metal oxide doping or modification were introduced into nitrogen-doped TiO_2 by acting as electron (or hole) traps to decrease the e^-/h^+ pair recombination rate and subsequently increase the lifetime of charge carriers [26–30], the intrinsic deficiency still exists in these co-doped TiO_2 systems.

Computer modeling and simulation provide great assistance to direct the development of materials with novel structure and properties. First-principles calculation method is now extensively used in the understanding of the structure and properties of materials, and subsequent material design [31–34]. In a recent study by Gai et al. [35], first-principles band structure calculations suggested that a passivated *n–p* co-doping approach, which involved doping both the donor (*n*) and accepter (*p*) dopants to TiO_2 , could reduce the band gap of TiO_2 to impart it the visible light photocatalytic activity. Charge compensations formed between excessive negative charges from the donor dopants and excessive positive charges from the accepter dopants, and passivated defect bands will not

* Corresponding author at: 72 Wenhua Road, Shenyang, Liaoning Province, 110016, PR China. Tel.: +86 24 83978028; fax: +86 24 23971215.

E-mail addresses: qili@imr.ac.cn, qiliuic@gmail.com (Q. Li).

be effective as carrier recombination centers. Thus, the passivated *n*-*p* co-doping approach may largely enhance the photocatalytic performance of TiO_2 under visible light illumination. One effective passivated *n*-*p* co-doping system predicted in their work was niobium and nitrogen co-doping, which could reduce the band gap of TiO_2 while uplifting the conducting band minimum (CBM). The calculation result also predicted that the passivated *n*-*p* co-doping were more stable than either dopant.

We report here the successful passivated *n*-*p* co-doping of niobium and nitrogen into self-organized TiO_2 nanotube arrays, which demonstrated largely enhanced photocatalytic performance under visible light illumination compared with TiO_2 nanotube arrays doped with either dopant. Unlike nitrogen doping, incorporating metal ions into TiO_2 nanotube arrays uniformly is difficult during anodization or through post-anodization treatments. For example, niobium doping was mostly concentrated within the near-surface region in the anodization of titanium using a fluoroniobate complex as both the niobium and fluoride sources in a recent report [36]. However, niobium could form a single phase Ti–Nb alloy with titanium by a solid-solution heat treatment followed with a quench treatment over a wide composition range [37–40], which provides the possibility for niobium to be incorporated into the nanotube arrays when the Ti–Nb alloy was anodized in fluoride-based electrolyte solutions [41,42]. The wide range of Nb content in the single phase Ti–Nb alloy allows the experimental investigation into the effect of the *n*-type Nb dopant content on the *p*-type nitrogen doping by heat treating in a flow of ammonia. It was found that the nitrogen doping concentration increased with the increase of the Nb content although the nitrogen doping condition was the same for all the samples, which suggests that the interaction between Nb dopant and N dopant is beneficial to the nitrogen doping process and the subsequent enhancement of the visible light response and photocatalytic activity under visible light illumination of niobium and nitrogen co-doped TiO_2 nanotube arrays.

2. Experimental

2.1. Synthesis of $\text{Ti}_{1-x}\text{Nb}_x\text{ON}$ nanotube arrays

$\text{Ti}_{1-x}\text{Nb}_x$ (*x*: Nb atomic ratio of 0.01, 0.025, 0.05, and 0.1) alloys were obtained by smelting Ti and Nb together at proper Ti/Nb atomic ratios in a non consumable electrode arc furnace in Ar atmosphere. The alloys were held at 1000 °C for 4 h followed with a quench in salt water (15% NaCl) to room temperature at about 2000 °C/s to obtain a single-phase microstructure. Self-organized nanotube arrays were synthesized by anodization of $\text{Ti}_{1-x}\text{Nb}_x$ alloy sheet at room temperature. Before anodization, $\text{Ti}_{1-x}\text{Nb}_x$ alloy sheets were degreased by sonicating in ethanol, acetone and deionized (DI) water, respectively, followed by rinsing with DI water and blow-drying under nitrogen purge. The anodization was conducted in a solution consisting of 0.25 M HF and 0.2 M ammonia (pH ~3.5) at 20 V for 30 min in a two-electrode electrochemical system (2 cm separation) with a platinum foil (0.1 mm thick, 99.9%) as the cathode. Magnetic stirring was adopted during the anodization to facilitate the diffusion of ions. After anodization, the obtained samples were rinsed in DI water and dried in air. To introduce nitrogen doping and create crystallized samples, some of these as-formed samples were then calcinated in a flow of ammonia gas at 450 °C for 0.5 h. The obtained samples were named as $\text{Ti}_{1-x}\text{Nb}_x\text{ON}$ to represent the atomic ratio of Ti and Nb in the initial alloy sheets. Some of these as-formed samples were then calcinated in a flow of O₂ gas at 450 °C for 0.5 h, and the obtained samples were named as $\text{Ti}_{1-x}\text{Nb}_x\text{O}_2$. For comparison purpose, pure titanium sheets (0.25 mm in thickness, 99.99% in purity) were anodized

under the same conditions. Some of these obtained nanotube samples were annealed in a flow of ammonia gas at 450 °C for 0.5 h, and the obtained samples were named as TiON. Some of these obtained nanotube samples were annealed in a flow of O₂ at 450 °C for 0.5 h, and the obtained samples were named as TiO_2 .

2.2. Characterization of $\text{Ti}_{1-x}\text{Nb}_x\text{ON}$ nanotube arrays

The surface morphology, microstructure and composition of samples were investigated using a SUPRA35 field emission scanning electron microscopy (FESEM) and a Tecnai F30 transmission electron microscopy (TEM) equipped with an energy dispersive spectrometer (EDS). Phase structures were analyzed by the glancing angle X-ray diffraction (GAXRD) on a D/MAX-2004 X-ray diffractometer with Cu K α ($\lambda = 0.15418 \text{ nm}$) radiation at 45 kV and 40 mA. A glancing angle of 5° was used for all the samples. XPS measurements were made on an ESCALAB250 X-ray photo-electron spectrometer with an Al K α anode (1486.6 eV photon energy, 300 W). The binding energy shift due to relative surface charging was corrected by using 284.6 eV as the C 1s peak as an internal standard. Their UV-vis spectra were measured on a Shimadzu UV-2550 spectrophotometer in diffusive reflectance mode.

2.3. Photoelectrochemical test

The monochromatic photocurrent density as a function of wavelength for nanotube array samples was measured under monochromatic light illumination of xenon lamp using a WDG30-Z grating monochromator. The measurements were performed in a three-electrode configuration in 0.2 M Na₂SO₄ solution, with platinum as the counter electrode and Ag/AgCl electrode as the reference electrode, by the CHI 660B electrochemical workstation. The *I*–*V* curves of the electrodes were measured with the same electrochemical system. An AM1.5G simulated sunlight (100 mW/cm²) was used as the light source, and a glass filter was used to eliminate light with wavelength less than 400 nm.

2.4. Photocatalytic degradation of methylene blue

Methylene blue was used as a model organic pollutant for photocatalytic degradation experiment under visible light illumination. All samples had the same area of 4 cm². They were placed at the bottom of 8 mm Petri dishes, and 6 mL of MB solution (2 ppm) was then added into the Petri dish. The covered Petri dish was illuminated by a metal halogen desk lamp with a glass filter. Zero light intensity was detected below 400 nm. The light intensity striking the samples was at ca. 3.0 mW/cm². The visible-light illumination time varied from 15 min to 2 h. After the visible light illumination, the light absorption of the clear solution was measured by a Shimadzu UV-2550 spectrophotometer. The remaining percentage of MB in the solution was calculated by the ratio between the light absorptions of treated and untreated MB solutions. For each illumination time (15 min, 30 min, 1 h, and 2 h, respectively), the same nanotube array sample of each kind was used repeatedly for the photocatalytic degradation of MB under visible light illumination. After one reaction, the nanotube sample was washed with DI water and dried by the nitrogen purge before it was used for the photocatalytic MB degradation of another illumination time. No damage was observed on these nanotube arrays during the repeated photocatalytic MB degradation processes, which demonstrated that these $\text{Ti}_{1-x}\text{Nb}_x\text{ON}$ nanotube arrays were stable under visible light. For comparison purpose, we also examined MB adsorption on these nanotube arrays in dark, and the MB degradation with only visible light illumination.

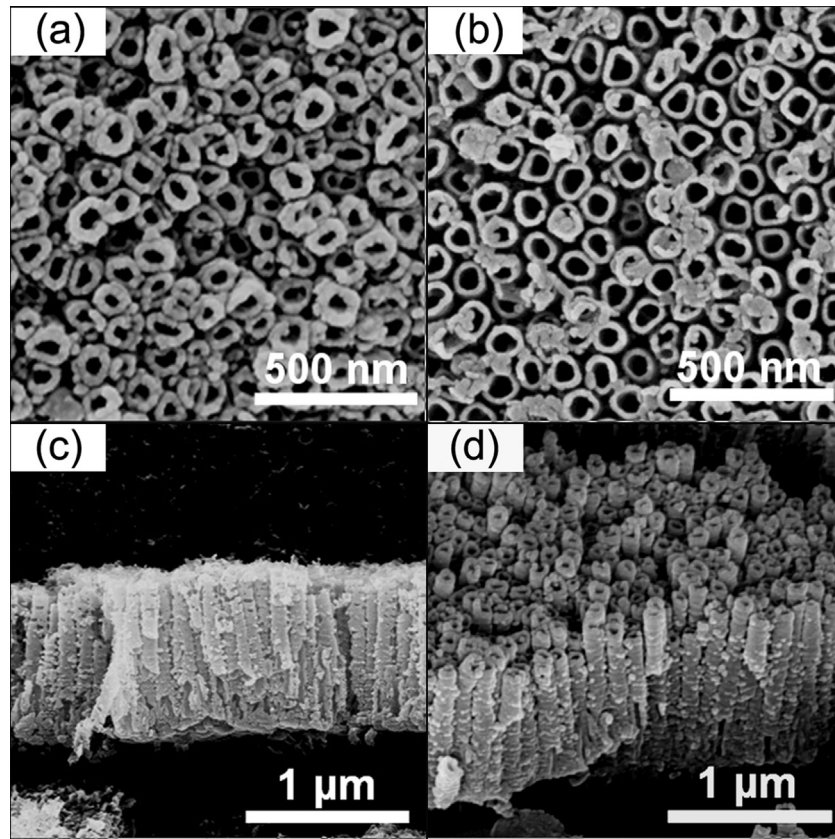


Fig. 1. (a) and (b) Top-view FESEM images of TiON and $\text{Ti}_{0.9}\text{Nb}_{0.1}\text{ON}$ nanotube arrays, respectively. (c) and (d) Cross-sectional view FESEM images of TiON and $\text{Ti}_{0.9}\text{Nb}_{0.1}\text{ON}$ nanotube arrays, respectively.

3. Results and discussion

3.1. Morphology, microstructure and composition of $\text{Ti}_{0.9}\text{Nb}_{0.1}\text{ON}$ nanotube arrays

$\text{Ti}_{1-x}\text{Nb}_x$ (x : Nb atomic ratio) alloys were obtained by smelting Ti and Nb together at proper Ti/Nb atomic ratios, and quenched from 1000 °C to room temperature to obtain a single-phase microstructure. Self-organized nanotube arrays were synthesized by anodization of $\text{Ti}_{1-x}\text{Nb}_x$ alloy sheet at room temperature. The $\text{Ti}_{0.9}\text{Nb}_{0.1}\text{ON}$ nanotube array sample was chosen as a representative for the demonstration of the characterization and properties of $\text{Ti}_{1-x}\text{Nb}_x\text{ON}$ nanotube arrays. **Fig. 1** shows the FESEM images of the nanostructures formed by anodizing pure Ti foil and $\text{Ti}_{0.9}\text{Nb}_{0.1}$ sheets, respectively. Both samples were composed of nanotube array structures. **Fig. 1a** and b shows the top views of TiON and $\text{Ti}_{0.9}\text{Nb}_{0.1}\text{ON}$ samples, respectively. The average diameters of these nanotubes were both ~ 100 nm. The average wall thicknesses were ~ 25 nm and ~ 20 nm for TiON and $\text{Ti}_{0.9}\text{Nb}_{0.1}\text{ON}$ samples, respectively. **Fig. 1c** and d shows the cross-section images of TiON and $\text{Ti}_{0.9}\text{Nb}_{0.1}\text{ON}$ samples, respectively. The thicknesses of these nanotube array films were both ~ 1 μm . The morphology observation results indicate that nanotube arrays could be formed when Nb existed in the metal sheet.

Fig. 2 demonstrates the GAXRD patterns of TiO_2 , $\text{Ti}_{1-x}\text{Nb}_x\text{O}_2$, TiON, and $\text{Ti}_{0.9}\text{Nb}_{0.1}\text{ON}$ nanotube arrays. Peaks of alpha titanium in these XRD patterns came from the metal substrates under these nanotube arrays. The differences of alpha Ti diffraction peak intensities in these samples could be attributed to the microstructural differences between pure Ti and $\text{Ti}_{1-x}\text{Nb}_x$ sheets in crystal size and texture. **Fig. 2a** compares the GAXRD patterns of TiO_2 and $\text{Ti}_{1-x}\text{Nb}_x\text{O}_2$ nanotube arrays with various Nb contents, and **Fig. 2b**

shows their anatase (101) peaks at a higher magnification. All samples contained only anatase phase, and no diffraction peak of niobium species was observed for $\text{Ti}_{1-x}\text{Nb}_x\text{O}_2$ nanotube arrays. The anatase (101) diffraction peak position of TiO_2 was 25.32°, while that of $\text{Ti}_{1-x}\text{Nb}_x\text{O}_2$ gradually decreased to 25.11° when the Nb content in the alloy sheet was 10%. The atomic radius of Nb^{5+} is 0.64 Å, while that of Ti^{4+} is 0.605 Å [43]. The closeness of their sizes makes it not difficult for Nb^{5+} to replace Ti^{4+} in the anatase lattice, which could slightly increase the lattice spacing and subsequently decrease the diffraction peak position as observed in **Fig. 2a** and b. From the absence of diffraction peaks of niobium species and the decrease of (101) peak position in $\text{Ti}_{1-x}\text{Nb}_x\text{O}_2$ nanotube arrays, the XRD analysis results suggest that Nb^{5+} may be doped into anatase lattice by replacing Ti^{4+} cations in the anatase lattice [38]. **Fig. 2c** compares the GAXRD patterns of TiO_2 , TiON, and $\text{Ti}_{0.9}\text{Nb}_{0.1}\text{ON}$ nanotube arrays, and **Fig. 2d** shows their anatase (101) peaks at a higher magnification. Similar results were observed when nitrogen doping was introduced, and the diffraction peak position shift could still be attributed mainly to the Nb-doping.

Fig. 3 shows the TEM analysis results of $\text{Ti}_{0.9}\text{Nb}_{0.1}\text{ON}$ nanotube arrays. **Fig. 3a** shows the TEM image of these nanotube arrays. Clear nanotube structure was observed, which is in accordance with the FESEM observations. Their SAED pattern (**Fig. 3b**) showed only anatase structure and no niobium diffraction ring could be observed. This observation is in accordance with the GAXRD analysis results, indicating the doping of niobium into anatase lattice. EDS analysis was conducted on the square area in **Fig. 3a**. The Ti/Nb atomic ratio was determined at 5.5:1, which confirms the existence of Nb in the nanotube arrays. The obtained Ti/Nb atom ratio is lower than that of the original $\text{Ti}_{0.9}\text{Nb}_{0.1}$ alloy (9:1), which indicates that Nb is more stable and could remain its existence in these samples easily under the anodization process, in accordance with the

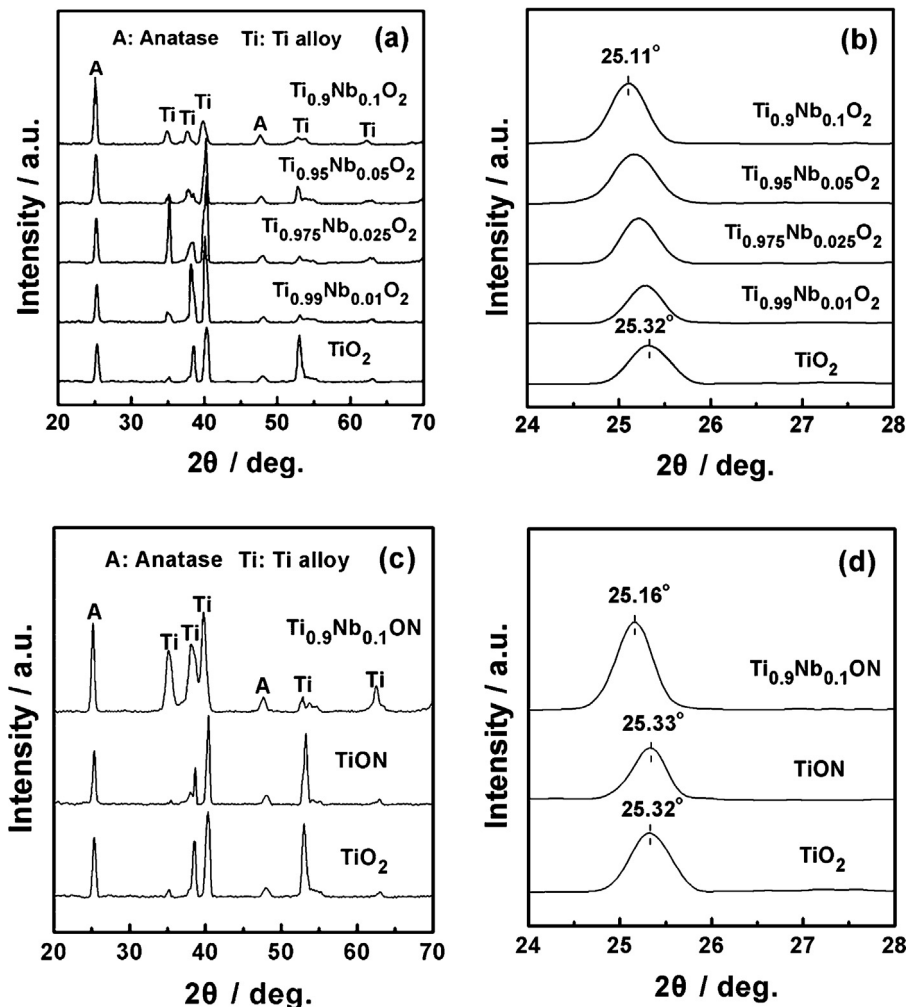


Fig. 2. (a) Glancing angle X-ray diffraction (GAXRD) patterns of TiO_2 and $\text{Ti}_{1-x}\text{Nb}_x\text{O}_2$ nanotube arrays. (b) GAXRD (101) peaks of TiO_2 and $\text{Ti}_{1-x}\text{Nb}_x\text{O}_2$ nanotube arrays. (c) GAXRD patterns of TiO_2 , TiON, and $\text{Ti}_{0.9}\text{Nb}_{0.1}\text{ON}$ nanotube arrays. (d) GAXRD (101) peaks of TiO_2 , TiON, and $\text{Ti}_{0.9}\text{Nb}_{0.1}\text{ON}$ nanotube arrays.

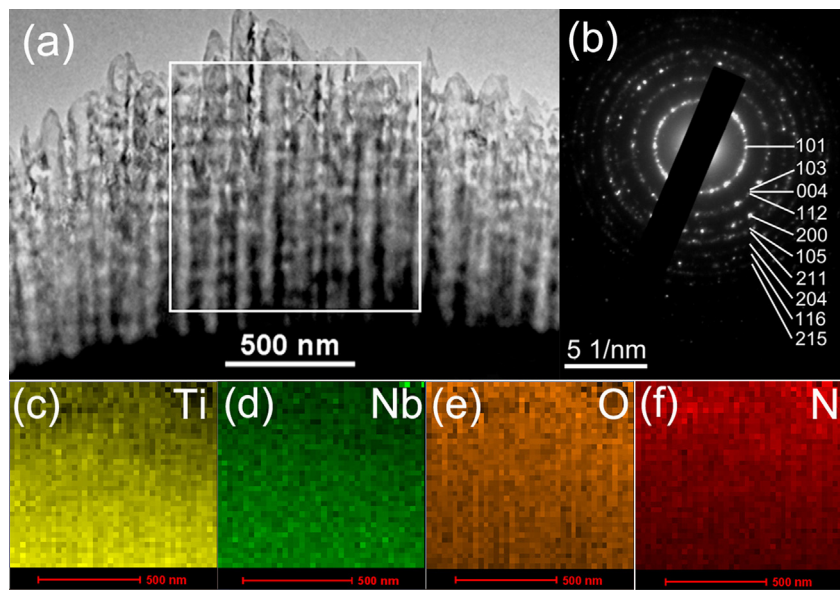


Fig. 3. (a) and (b) TEM image and SAED patterns of $\text{Ti}_{0.9}\text{Nb}_{0.1}\text{ON}$ nanotube arrays, respectively. (c)–(f) The distribution map of Ti, Nb, O, and N elements in $\text{Ti}_{0.9}\text{Nb}_{0.1}\text{ON}$ nanotube arrays, respectively.

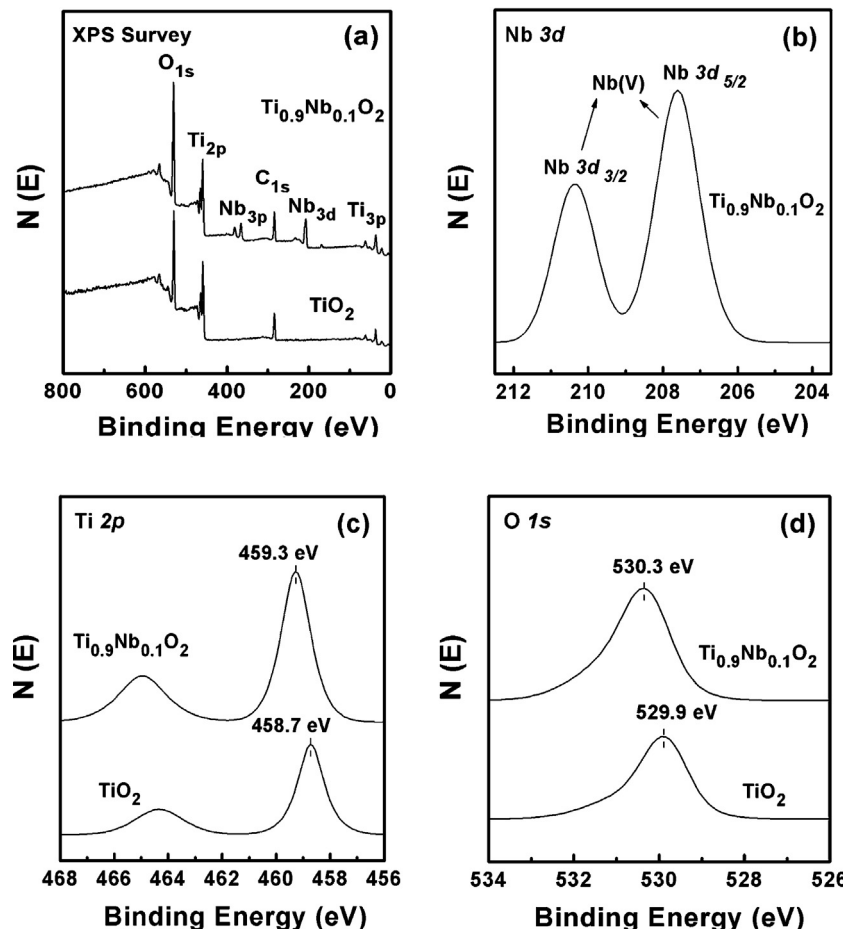


Fig. 4. (a) Representative XPS survey spectra of TiO_2 and $\text{Ti}_{0.9}\text{Nb}_{0.1}\text{O}_2$ nanotube arrays. (b) High-resolution XPS scan over Nb 3d peak of $\text{Ti}_{0.9}\text{Nb}_{0.1}\text{O}_2$ nanotube arrays. (c) and (d) High-resolution XPS scans over Ti 2p and O 1s peaks of TiO_2 , and $\text{Ti}_{0.9}\text{Nb}_{0.1}\text{O}_2$ nanotube arrays, respectively.

report by Ghicov et al. [41]. Fig. 3c–f shows the distribution map of Ti, Nb, O, and N elements in the square area surrounded by the white box in Fig. 3a. Fig. 3c demonstrates that the Ti distribution map at the bottom part of these nanotubes is brighter than that at the top part, which indicates lower titanium content at the top part of these nanotubes. This observation is in accordance with the observed lower Ti/Nb atomic ratio at 5.5:1 because Nb is more stable. The top part of these nanotubes was exposed to the electrolyte for a longer time, thus leading to the reduced titanium content. Fig. 3d and e demonstrates that Nb and O elements distributed relatively uniformly in these nanotube arrays. From Fig. 3f, N element existed in the whole $\text{Ti}_{0.9}\text{Nb}_{0.1}\text{ON}$ nanotube arrays, which verifies the introduction of nitrogen into the nanotube structure. The top part of Fig. 3f is relatively brighter than the bottom part, indicating a higher N content in this region. This observation could be easily understood from the nitrogen doping process utilized in this study, in which the contact of nanotubes with NH_3 molecules is the key step. The top part of these nanotubes had the best chance to contact with NH_3 molecules, which results in the higher nitrogen content. From the EDS analysis, the existence of Nb and N in $\text{Ti}_{0.9}\text{Nb}_{0.1}\text{ON}$ nanotube arrays was verified.

3.2. Niobium and nitrogen co-doping in $\text{Ti}_{0.9}\text{Nb}_{0.1}\text{ON}$ nanotube arrays

XPS analysis was used to obtain semiquantitative data on the chemical compositions of obtained samples. Fig. 4a shows the representative XPS survey spectra of TiO_2 and $\text{Ti}_{0.9}\text{Nb}_{0.1}\text{O}_2$ nanotube

arrays. Due to the widespread presence of carbon in the environment, C 1s peak was observed in both XPS survey spectra. The existence of Ti and O was clearly observed for both samples, and Nb 3d peak could be clearly observed for $\text{Ti}_{0.9}\text{Nb}_{0.1}\text{O}_2$ nanotube arrays. Fig. 4b shows the high-resolution XPS scan over Nb 3d for $\text{Ti}_{0.9}\text{Nb}_{0.1}\text{O}_2$ nanotube arrays, which indicates that the only chemical state of niobium in the sample is Nb^{5+} and no metallic Nb^0 could be found. Fig. 4c and d compares the high-resolution XPS scans over Ti 2p and O 1s peaks of TiO_2 and $\text{Ti}_{0.9}\text{Nb}_{0.1}\text{O}_2$ nanotube arrays, respectively. Compared with TiO_2 nanotube arrays, both Ti 2p and O 1s peaks of $\text{Ti}_{0.9}\text{Nb}_{0.1}\text{O}_2$ nanotube arrays were shifted toward higher binding energy, which could be attributed to the doping of Nb [44]. It had been demonstrated that the doping of some high valence transition metal ions (such as W^{6+} and Nb^{5+}) into TiO_2 could cause a positive shift of Ti 2p and O 1s peaks due to a certain level of electron drain from the Ti^{4+} in the oxide matrix [44–47].

Fig. 5a compares the representative XPS survey spectra of TiO_2 , TiON and $\text{Ti}_{0.9}\text{Nb}_{0.1}\text{ON}$ nanotube arrays. The existence of Ti and O was clearly observed for all samples, and Nb 3d peak could be clearly observed for $\text{Ti}_{0.9}\text{Nb}_{0.1}\text{ON}$ nanotube arrays. For TiON nanotube arrays, the N 1s peak was not obvious in its XPS survey spectrum, while N 1s peak could be easily identified in that of $\text{Ti}_{0.9}\text{Nb}_{0.1}\text{ON}$ nanotube arrays. Fig. 5b shows the high-resolution XPS scan over Nb 3d for $\text{Ti}_{0.9}\text{Nb}_{0.1}\text{ON}$ nanotube arrays, which indicates that the only chemical state of niobium in the sample is Nb^{5+} . From the Nb 3d peak position, it could also be concluded that most niobium was bound with oxygen in the sample due to the lack of

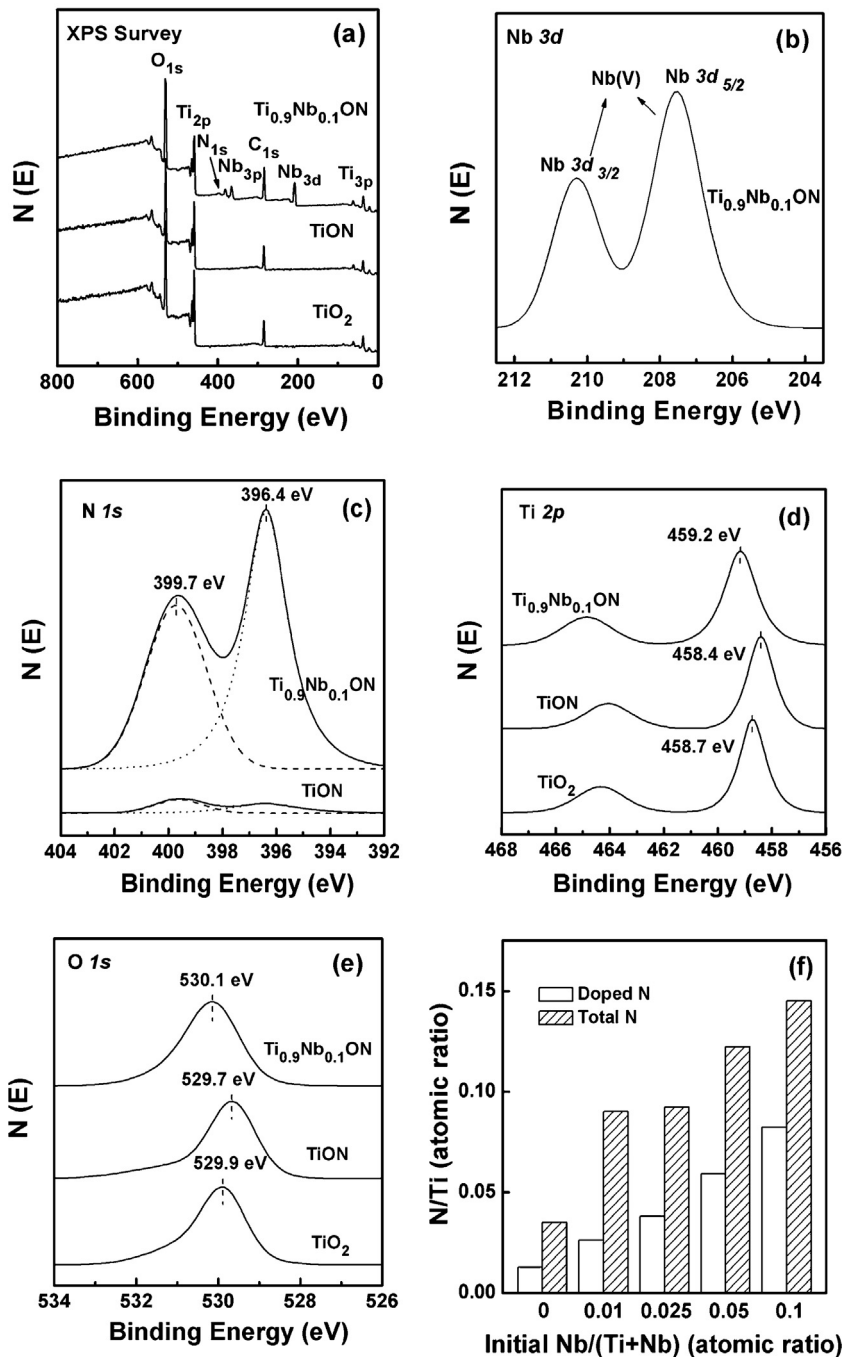


Fig. 5. (a) Representative XPS survey spectra of TiO_2 , TiON and $\text{Ti}_{0.9}\text{Nb}_{0.1}\text{ON}$ nanotube arrays. (b) High-resolution XPS scan over Nb 3d peaks of $\text{Ti}_{0.9}\text{Nb}_{0.1}\text{ON}$ nanotube arrays. (c) and (d) High-resolution XPS scans over Ti 2p and O 1s peaks of TiO_2 , TiON and $\text{Ti}_{0.9}\text{Nb}_{0.1}\text{ON}$ nanotube arrays, respectively. (e) High-resolution XPS scans over N 1s peaks of TiON and $\text{Ti}_{0.9}\text{Nb}_{0.1}\text{ON}$ nanotube arrays, respectively. (f) The N/Ti atomic ratios in TiON and $\text{Ti}_{1-x}\text{Nb}_x\text{ON}$ ($x = 0.01, 0.25, 0.05, 0.1$) nanotube arrays, respectively.

peaks near 204 eV [48,49] for Nb-N bonds. Fig. 5c compares the high-resolution XPS scans over N 1s peak of TiON and $\text{Ti}_{0.9}\text{Nb}_{0.1}\text{ON}$ nanotube arrays. For both samples, their N 1s spectra could be best fitted as a combination of two peaks at 399.70 and 396.40 eV. The N 1s peak near 400 eV could be assigned to N atoms from molecularly adsorbed N-containing compounds, while the N 1s peak near 396.5 eV could be attributed to N atoms that replace O atoms in TiO_2 crystal lattice and form Ti–N bonds [6,50]. Thus, clear evidence was obtained to verify the doping of nitrogen in these nanotube arrays. However, the N 1s peak signal intensity of $\text{Ti}_{0.9}\text{Nb}_{0.1}\text{ON}$ nanotube arrays is much stronger than that of TiON nanotube arrays, indicating a much higher N content in $\text{Ti}_{0.9}\text{Nb}_{0.1}\text{ON}$

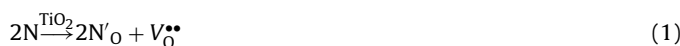
nanotube arrays. Fig. 5d and e compares the high-resolution XPS scans over Ti 2p and O 1s peaks of TiO_2 , TiON , and $\text{Ti}_{0.9}\text{Nb}_{0.1}\text{ON}$ nanotube arrays, respectively. Compared with that of TiO_2 nanotube arrays, a clear shift toward lower binding energy was found for both Ti 2p and O 1s peaks of TiON nanotube arrays, which also indicates the successful incorporation of nitrogen dopants into TiO_2 lattice [51–54]. For $\text{Ti}_{0.9}\text{Nb}_{0.1}\text{ON}$ nanotube arrays, however, both Ti 2p and O 1s peaks were shifted toward higher binding energy although the nitrogen doping concentration is much higher in $\text{Ti}_{0.9}\text{Nb}_{0.1}\text{ON}$ nanotube arrays compared with TiON nanotube arrays. This observation could be attributed to the high Nb doping concentration in this sample [44], which overcomes the effect from nitrogen

doping. XPS analysis results here with the XRD and TEM analysis results confirm the successful co-doping of niobium and nitrogen into the anatase lattice of TiO_2 nanotube arrays by our synthesis process.

The effect of niobium doping on the nitrogen doping in this material system was examined by comparing the total nitrogen/doped nitrogen concentrations in the $\text{Ti}_{1-x}\text{Nb}_x\text{ON}$ nanotube array samples synthesized from a series of $\text{Ti}_{1-x}\text{Nb}_x$ (x at 0.01, 0.025, 0.05, and 0.1, respectively) alloys under same synthesis conditions. The increased Nb amount in the $\text{Ti}_{1-x}\text{Nb}_x$ alloy increased the Nb doping concentration in the $\text{Ti}_{1-x}\text{Nb}_x\text{ON}$ nanotube array samples. The XPS analysis demonstrated that the Nb/Ti atomic ratio in $\text{Ti}_{1-x}\text{Nb}_x\text{ON}$ nanotube array samples increased from 1:33 for $\text{Ti}_{0.99}\text{Nb}_{0.01}\text{ON}$ to 1:5.5 for $\text{Ti}_{0.9}\text{Nb}_{0.1}\text{ON}$. Fig. 5f summarizes the N/Ti atomic ratios in these samples. With the increase of Nb doping, both the total nitrogen and the doped nitrogen concentrations increased dramatically. When there was no Nb doping, the total N/Ti and doped N/Ti atomic ratios of TiON nanotube arrays were 0.035 and 0.013, respectively. However, the total N/Ti and doped N/Ti atomic ratios of $\text{Ti}_{0.9}\text{Nb}_{0.1}\text{ON}$ nanotube arrays increased to 0.145 and 0.082, representing an increase of 314% and 531%, respectively. It is evident that the Nb doping in TiO_2 could significantly enhance the nitrogen doping process. The doped-N/Nb ratio for $\text{Ti}_{0.9}\text{Nb}_{0.1}\text{ON}$ nanotube arrays was $\sim 0.451:1$. For the passivated $n-p$ co-doping of niobium and nitrogen to TiO_2 , the oxygen vacancy becomes the lowest when the doped Nb and N contents are the same. Thus, the nitrogen-doping process could be further optimized to increase the nitrogen dopant concentration for the optimized photocatalytic performance.

The enhancement mechanism might be explained as follows. The passivated $n-p$ co-doping process had two steps. In the first step, Nb^{5+} was doped into TiO_2 to replace Ti^{4+} during the anodization of $\text{Ti}_{1-x}\text{Nb}_x$ alloy. Due to its higher valence than Ti^{4+} , the replacement of Ti^{4+} by Nb^{5+} could lead to the formation of acid centers with a positive charge on the prior Ti^{4+} sites substituted by Nb^{5+} [38,51]. In the second step, the nitrogen doping was conducted by the heat treatment of Nb-doped TiO_2 nanotube arrays in NH_3 atmosphere, which makes the adsorption of NH_3 onto anatase surface the prerequisite. For NH_3 , there is a lone-electron pair outside of N atom. Thus, an attraction exists between NH_3 and acid centers of Nb-doped TiO_2 surface from the Coulomb force, which could promote its adsorption onto the surface of Nb-doped TiO_2 . The enhanced NH_3 adsorption could subsequently increase the total N content in Nb and N co-doped TiO_2 compared with TiON, and provide a better chance for nitrogen to be doped into the anatase lattice when Nb-doping is present.

The nitrogen doping into TiO_2 by replacing O atoms could be described using formula (1):



After the doping process, a new equilibrium in the material system will be re-established following the principle of minimum energy. As an acceptor dopant, N dopant will cause the formation of oxygen vacancy, which increases the system's energy and makes it difficult for nitrogen dopants to replace O atoms in the anatase lattice. Due to its higher valence than Ti^{4+} , the replacement of Ti^{4+} by Nb^{5+} could reduce the oxygen vacancy amount [55]. So the doping of Nb^{5+} may decrease the system energy increase by consuming oxygen vacancies, which is likely to facilitate the N doping. Thus, the increase of Nb doping concentration in TiO_2 could increase the amount of nitrogen dopant as observed in this series of samples. This experimental observation is in accordance with the calculation prediction by Gai et al. [35].

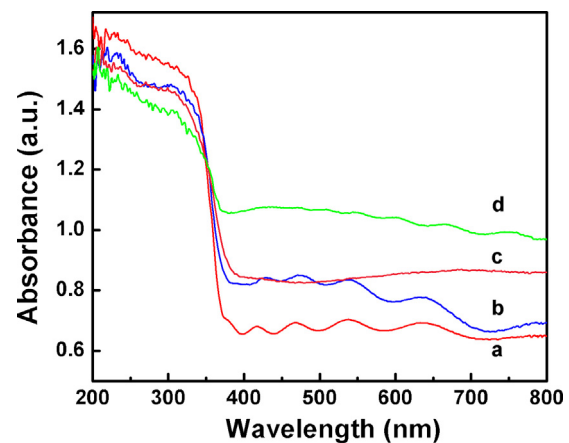


Fig. 6. Light absorbance of TiO_2 (a), TiON (b), $\text{Ti}_{0.9}\text{Nb}_{0.1}\text{O}_2$ (c), and $\text{Ti}_{0.9}\text{Nb}_{0.1}\text{ON}$ (d) nanotube arrays.

3.3. Optical properties of $\text{Ti}_{0.9}\text{Nb}_{0.1}\text{ON}$ nanotube arrays

The optical absorbances of nanotube array samples were determined from the diffuse reflectance measurements. Fig. 6 shows the light absorbance of TiO_2 , TiON, $\text{Ti}_{0.9}\text{Nb}_{0.1}\text{O}_2$, and $\text{Ti}_{0.9}\text{Nb}_{0.1}\text{ON}$ nanotube arrays, respectively. These nanotube array samples demonstrated light absorbance from UV to visible light region. Their observed high absorption tails into the visible light region may be partially attributed to light scatterings from metal substrates under the nanotube arrays. For TiO_2 nanotube arrays, their low visible light absorbance could be attributed to their specific nanotube architecture, which brings relatively higher crystal lattice distortion [7]. With a very small amount of nitrogen dopants (N/Ti atomic ratio of 0.013), TiON nanotube arrays demonstrated an enhanced visible light absorbance than TiO_2 nanotube arrays, which is expected and could be attributed to the nitrogen doping effect [15–19,51]. $\text{Ti}_{0.9}\text{Nb}_{0.1}\text{O}_2$ nanotube arrays also demonstrated an enhanced visible light absorbance than TiO_2 nanotube arrays, which is consistent with some previous reports [37,54]. Among all these samples, $\text{Ti}_{0.9}\text{Nb}_{0.1}\text{ON}$ nanotube arrays had the highest visible light absorbance, which could be attributed to the co-doping of niobium and nitrogen. Their largely enhanced visible light absorbance suggests that an enhanced photocatalytic performance could be expected.

3.4. Photoelectrochemical properties of $\text{Ti}_{0.9}\text{Nb}_{0.1}\text{ON}$ nanotube arrays

Fig. 6 demonstrated that the background absorbance from the metal substrate was high in the visible light range, which may affect the actual visible light response of these nanotube arrays. Thus, the photochemical response of these nanotube arrays were further examined. Fig. 7a shows the photocurrent spectra of TiO_2 , TiON, $\text{Ti}_{0.9}\text{Nb}_{0.1}\text{O}_2$, and $\text{Ti}_{0.9}\text{Nb}_{0.1}\text{ON}$ nanotube arrays under the irradiation of monochromatic light with various wavelengths, respectively. $\text{Ti}_{0.9}\text{Nb}_{0.1}\text{O}_2$ nanotube arrays demonstrated an enhanced visible light response than TiO_2 nanotube arrays, which was consistent with some previous reports [37,54]. The photocurrent density values of TiON nanotube arrays were also higher than that of TiO_2 nanotube arrays in the visible light range, which could be attributed to the nitrogen doping as an effective method to enhance the visible light response of TiO_2 [15–19,51]. $\text{Ti}_{0.9}\text{Nb}_{0.1}\text{ON}$ nanotube arrays demonstrated the best performance under visible light illumination, which should result from the enhancement of nitrogen-doping from the co-doping of niobium. Fig. 7b shows the band gap values determination of these nanotube arrays from the Tauc Plots

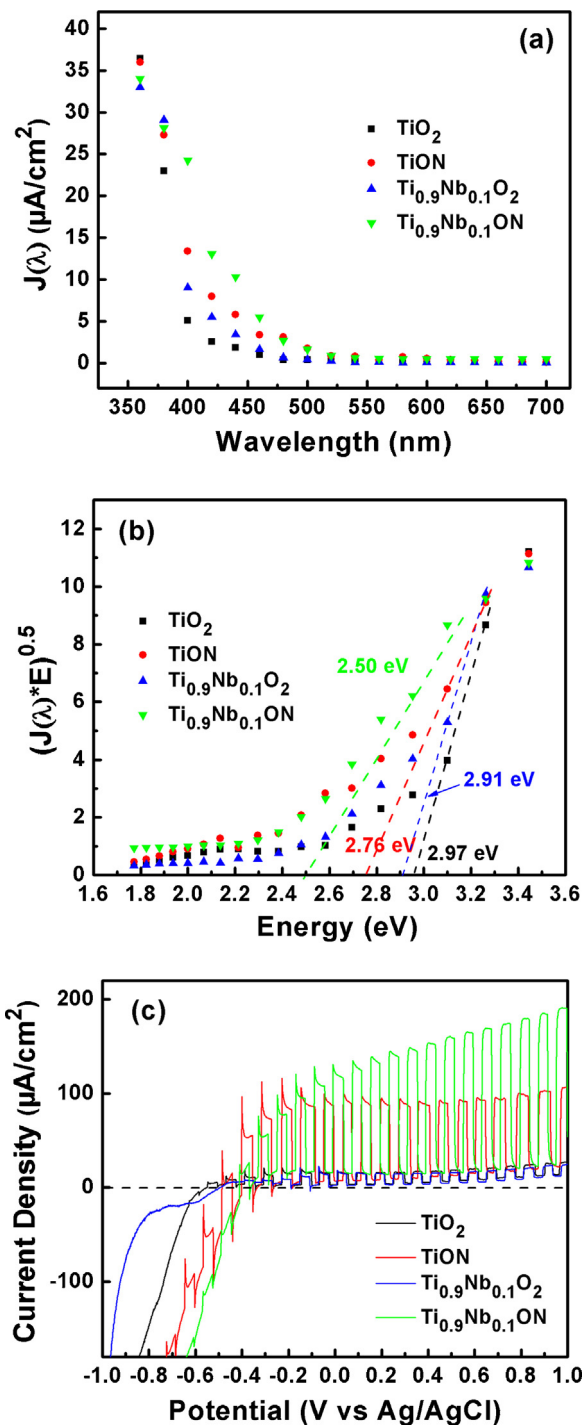


Fig. 7. (a) Photocurrent spectra of TiO_2 , TiON , $\text{Ti}_{0.9}\text{Nb}_{0.1}\text{O}_2$, and $\text{Ti}_{0.9}\text{Nb}_{0.1}\text{ON}$ nanotube arrays recorded at 0.3 V vs. Ag/AgCl under monochromatic light with various wavelength. (b) Tauc Plots ($(J(\lambda) \times h\nu)^{0.5}$ vs $h\nu$) of nanotube arrays constructed from photocurrent spectra in Fig. 6a. (c) I - V curves of TiO_2 , TiON , $\text{Ti}_{0.9}\text{Nb}_{0.1}\text{O}_2$ and $\text{Ti}_{0.9}\text{Nb}_{0.1}\text{ON}$ nanotube arrays under AM1.5G simulated sunlight ($100 \text{ mW}/\text{cm}^2$), and a filter was used to eliminate light with wavelength less than 400 nm.

$((J(\lambda) \times h\nu)^{0.5}$ vs $h\nu$) [56] constructed from Fig. 6a. The band gap values of TiO_2 , TiON , $\text{Ti}_{0.9}\text{Nb}_{0.1}\text{O}_2$, and $\text{Ti}_{0.9}\text{Nb}_{0.1}\text{ON}$ nanotube arrays were determined at 2.97 eV, 2.76 eV, 2.91 eV, and 2.58 eV, respectively.

Fig. 7c compares the photocurrent densities of those nanotube arrays under visible light illumination. It is clear that the nitrogen-doping is critical in this material system for an enhanced visible light response. Without nitrogen-doping, TiO_2 and $\text{Ti}_{0.9}\text{Nb}_{0.1}\text{O}_2$

nanotube arrays demonstrated much smaller photocurrents. Compared to $\text{Ti}_{0.9}\text{Nb}_{0.1}\text{ON}$ nanotube arrays, the decay of photocurrent on TiON without positive voltages was more obvious, indicating more recombination of electron-hole pairs [57]. $\text{Ti}_{0.9}\text{Nb}_{0.1}\text{ON}$ nanotube arrays demonstrated the highest visible light response enhancement to TiO_2 nanotube arrays. For example, the photocurrent densities on TiO_2 and $\text{Ti}_{0.9}\text{Nb}_{0.1}\text{ON}$ nanotube arrays were approximately $13 \mu\text{A}/\text{cm}^2$ and $165 \mu\text{A}/\text{cm}^2$ at the bias voltage of 1.0 V, respectively, representing an increase of about 12.7 times. The largely enhanced visible-light photoelectrochemical properties by passivated n - p co-doping of niobium and nitrogen into TiO_2 nanotube arrays absorbance suggested that a largely enhanced photocatalytic performance could be expected.

3.5. Photocatalytic degradation of methylene blue under visible light illumination

The photocatalytic activities of TiO_2 , TiON , $\text{Ti}_{0.9}\text{Nb}_{0.1}\text{O}_2$, and $\text{Ti}_{1-x}\text{Nb}_x\text{ON}$ nanotube arrays were examined by their degradation effects on a commonly used model pollutant, methylene blue (MB), under visible light illumination. For comparison purposes, we also examined MB adsorption on these nanotube arrays in dark, and MB degradation with only visible light illumination. The adsorption of MB on $\text{Ti}_{0.9}\text{Nb}_{0.1}\text{ON}$ nanotube arrays in the dark was the highest among these samples. After about 30 min interaction, the residual MB concentration reaches a plateau at ~88%. The adsorption of MB on other nanotube array samples was even lower. Thus, the adsorption of MB on these nanotube arrays only accounts for a very small portion in the decrease of MB concentration in the treated solutions. Fig. 8a summarizes the residual percentage of MB as a function of treatment time with various treatments. It is well-known that MB could absorb visible light and degrade itself under visible light illumination. This effect was also examined here. After 2 h interaction with visible light, ~84% MB still remained. Under the interactions with nanotube array samples under visible light illumination, the degradation of MB was largely accelerated. After 2 h interaction, the residual MB concentration of the solution treated with TiO_2 nanotube arrays dropped to ~68%, while the residue MB concentration of the solution treated with TiON nanotube arrays to ~57%. This observation demonstrated that nitrogen doping enhances the visible light photocatalytic activity of TiO_2 nanotube arrays. After 2 h interaction, the residual MB concentration of the solution treated with $\text{Ti}_{0.9}\text{Nb}_{0.1}\text{O}_2$ nanotube arrays dropped to ~42%. This observation demonstrated that niobium doping alone could enhance the photocatalytic activity of TiO_2 nanotube arrays, although the visible light response of $\text{Ti}_{0.9}\text{Nb}_{0.1}\text{O}_2$ nanotube arrays was not as high as that of TiON nanotube arrays. The enhanced MB degradation by $\text{Ti}_{0.9}\text{Nb}_{0.1}\text{O}_2$ nanotube arrays could be attributed to the additional electron trapping function of niobium doping, which decreases the e^-/h^+ pair recombination and subsequently enhances the photocatalytic activity. $\text{Ti}_{0.9}\text{Nb}_{0.1}\text{ON}$ nanotube arrays demonstrated the best degradation performance. After 2 h interaction, the residual MB concentration of the solution treated with $\text{Ti}_{0.9}\text{Nb}_{0.1}\text{ON}$ nanotube arrays dropped to ~12%. This largely enhanced photocatalytic activity could be attributed to their large nitrogen-doping enhancement from the niobium doping effect and the decreased e^-/h^+ pair recombination from the passivated n - p co-doping as discussed in prior sections. Thus, the photocatalytic degradation of MB results demonstrated that the successful passivated n - p co-doping of niobium and nitrogen of our approach largely enhanced the photocatalytic activity of TiO_2 nanotube arrays. Fig. 8b summarizes the residual percentage of MB as a function of treatment time with the treatment by $\text{Ti}_{1-x}\text{Nb}_x\text{ON}$ nanotube arrays with various Nb contents, compared with that by TiON nanotube arrays. With the increase of Nb content, the residual MB concentration decreased gradually, which further verified the photocatalytic performance

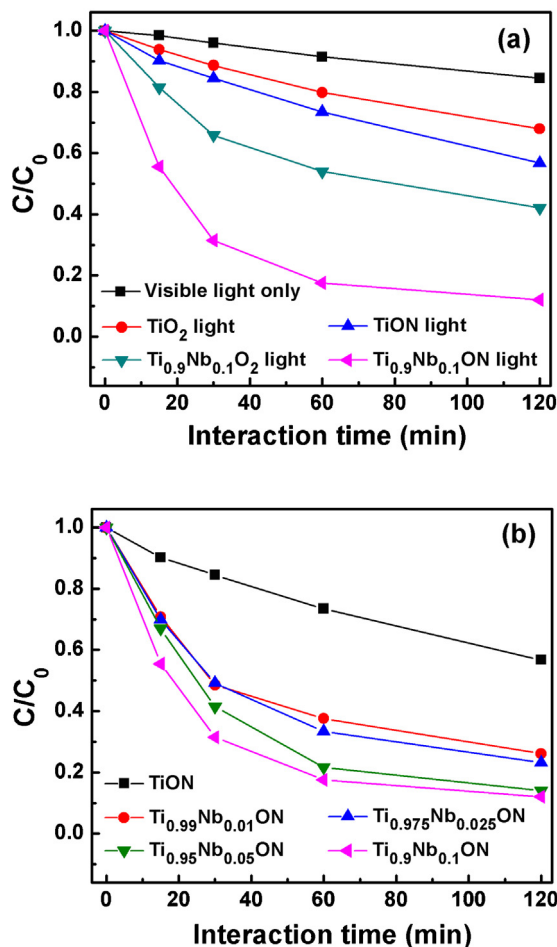


Fig. 8. Photo-degradation curves of MB on different nanotube arrays samples under visible light illumination: (a) TiO_2 , TiON , $\text{Ti}_{0.9}\text{Nb}_{0.1}\text{O}_2$, and $\text{Ti}_{0.9}\text{Nb}_{0.1}\text{ON}$. (b) $\text{Ti}_{1-x}\text{Nb}_x\text{ON}$ nanotube arrays.

enhancement from the successful passivated $n-p$ co-doping of niobium and nitrogen to TiO_2 nanotube arrays.

The slope of the MB degradation curve in Fig. 8a represents the MB degradation rate at certain treatment time. Generally, the degradation rate will gradually decrease because fewer and fewer MB molecules exist in the solution with the increase of the treatment time, which decreases their contact opportunity with nanotube arrays. Thus, the photocatalytic activity enhancement could be demonstrated quantitatively by the initial MB degradation rates under various treatments with the same initial MB concentration. Without nanotube arrays, the initial MB degradation rate under visible light illumination was $\sim 0.00133 \text{ min}^{-1}$. When TiO_2 nanotube arrays were present, its initial MB degradation rate was $\sim 0.00407 \text{ min}^{-1}$, representing an increase of $\sim 206\%$ to the self-degradation of MB under visible light illumination. The initial MB degradation rates by TiON , $\text{Ti}_{0.9}\text{Nb}_{0.1}\text{O}_2$, and $\text{Ti}_{0.9}\text{Nb}_{0.1}\text{ON}$ nanotube arrays were $\sim 0.00653 \text{ min}^{-1}$, $\sim 0.01233 \text{ min}^{-1}$, and $\sim 0.02967 \text{ min}^{-1}$, respectively, representing an increase of $\sim 60\%$, 203% , and 629% , respectively, to the initial MB degradation rate by TiO_2 nanotube arrays under visible light illumination. From the initial MB degradation rate analysis, it is evident that the passivated $n-p$ co-doping of niobium and nitrogen largely enhanced the photocatalytic activity of TiO_2 nanotube arrays under visible light illumination, compared with doping with either dopant.

Due to the different experimental conditions in various research works, it is difficult to compare the photocatalytic performances reported here vs. those in literatures directly. Thus, we chose to

compare the magnitude of the improvement in reference to pure TiO_2 . In a recent report on Zr and N co-doped TiO_2 nanotube arrays [58], the Zr and N co-doped TiO_2 nanotube arrays demonstrated an increase of only $\sim 46\%$ to TiO_2 nanotube arrays on the initial rhodamine B degradation rate under visible light illumination. In the study on PdO-modified N and F co-doped TiO_2 nanotube arrays [5,10], the PdO-modified N and F co-doped TiO_2 nanotube arrays demonstrated an increase of $\sim 281\%$ to TiO_2 nanotube arrays on the initial MB degradation rate under visible light illumination. However, our current study demonstrated that $\text{Ti}_{0.9}\text{Nb}_{0.1}\text{ON}$ nanotube arrays had a much larger increase of $\sim 629\%$ to TiO_2 nanotube arrays on the initial MB degradation rate under visible light illumination. As demonstrated previously [29,58–61], PdO-modification with nitrogen doping could largely enhance the photocatalytic performance of TiO_2 under visible light illumination. Thus, it is clear that the passivated $n-p$ co-doping of niobium and nitrogen is superior to either PdO-modification with nitrogen doping or Zr and N co-doping on the improvement of the photocatalytic performance of TiO_2 under visible light illumination, which is in accordance with the computational analysis. Thus, the passivated $n-p$ co-doping approach may become a very promising doping choice for TiO_2 -based photocatalysts.

4. Conclusions

In summary, passivated $n-p$ co-doping of niobium and nitrogen was successfully incorporated into self-organized TiO_2 nanotube arrays by anodizing Ti-Nb alloys, followed with the heat treatment in a flow of ammonia gas. Single phase $\text{Ti}_{1-x}\text{Nb}_x$ alloys offered a unique opportunity to explore Nb doping, over a wide compositional range, of titanium oxide photocatalyst. The presence of Nb dopant in TiO_2 nanotube arrays was found to enhance both the adsorption of NH_3 molecules on the TiO_2 nanotube and the subsequent nitrogen doping into the TiO_2 nanotube. The resulting Nb/N co-doped TiO_2 nanotube arrays demonstrated a largely enhanced visible light response and visible-light-activated photocatalytic activity than TiO_2 nanotube arrays or TiO_2 nanotube arrays with either dopant. The passivated $n-p$ co-doping approach may also be applied to other material systems and promise a wide range of technical applications.

Acknowledgements

This study was supported by the National Natural Science Foundation of China (Grant No. 51102246), the Knowledge Innovation Program of Institute of Metal Research, Chinese Academy of Sciences (Grant No. Y0N5A111A1), the Youth Innovation Promotion Association, Chinese Academy of Sciences (Grant No. Y2N5711171), and the Scientific Research Foundation for the Returned Overseas Chinese Scholars, State Education Ministry, PR China.

References

- [1] D. Gong, C.A. Grimes, O.K. Varghese, W. Hu, R.S. Singh, Z. Chen, E.C. Dickey, *J. Mater. Res.* 16 (2001) 3331–3334.
- [2] G.K. Mor, O.K. Varghese, M. Paulose, N. Mukherjee, C.A. Grimes, *J. Mater. Res.* 18 (2003) 2588–2593.
- [3] O.K. Varghese, D. Gong, M. Paulose, K.G. Ong, E.C. Dickey, C.A. Grimes, *Adv. Mater.* 15 (2003) 624–627.
- [4] J.M. Macak, H. Tsuchiya, P. Schmuki, *Angew. Chem. Int. Ed.* 44 (2005) 2100–2102.
- [5] Q. Li, J.K. Shang, *Environ. Sci. Technol.* 43 (2009) 8923–8929.
- [6] C. Ruan, M. Paulose, O.K. Varghese, G.K. Mor, C.A. Grimes, *J. Phys. Chem. B* 109 (2005) 15754–15759.
- [7] G.K. Mor, O.K. Varghese, M. Paulose, C.A. Grimes, *Adv. Funct. Mater.* 15 (2005) 1291–1296.
- [8] G.K. Mor, K. Shankar, M. Paulose, O.K. Varghese, C.A. Grimes, *Nano Lett.* 6 (2006) 215–218.

[9] Y. Liu, B. Zhou, J. Bai, J. Li, J. Zhang, Q. Zheng, X. Zhu, W. Cai, *Appl. Catal. B: Environ.* 89 (2009) 142–148.

[10] Q. Li, J.K. Shang, *Environ. Sci. Technol.* 44 (2010) 3493–3499.

[11] Y. Liu, J. Li, B. Zhou, H. Chen, Z. Wang, W. Cai, *Chem. Commun.* 47 (2011) 10314–10316.

[12] J. Orenstein, A.J. Millis, *Science* 288 (2000) 468–474.

[13] S.C. Erwin, L.J. Zu, M.I. HafTEL, A.L. Efros, T.A. Kennedy, D.J. Norris, *Nature* 436 (2005) 91–94.

[14] D.J. Norris, A.L. Efros, S.C. Erwin, *Science* 319 (2008) 1776–1779.

[15] R. Asahi, T. Morikawa, T. Ohwaki, K. Aoki, Y. Taga, *Science* 293 (2001) 269–271.

[16] H. Irie, Y. Watanabe, K. Hashimoto, *J. Phys. Chem. B* 107 (2003) 5483–5486.

[17] T. Umebayashi, T. Yamaki, H. Itoh, K. Asai, *Appl. Phys. Lett.* 81 (2002) 454–456.

[18] J.C. Yu, J.G. Yu, W.K. Ho, Z.T. Jiang, L.Z. Zhang, *Chem. Mater.* 14 (2002) 3808–3816.

[19] G.R. Torres, T. Lindgren, J. Lu, C.G. Granqvist, S.E. Lindquist, *J. Phys. Chem. B* 108 (2004) 5995–6003.

[20] A. Kubacka, G. Colón, M. Fernández-García, *Catal. Today* 143 (2009) 286–292.

[21] W. Choi, A. Termin, M.R. Hoffmann, *J. Phys. Chem. B* 98 (1994) 13669–13679.

[22] E. Borgarello, J. Kiwi, M. Grätzel, E. Pelizzetti, M. Visca, *J. Am. Chem. Soc.* 104 (1982) 2996–3002.

[23] J.M. Herrmann, J. Disdier, P. Pichat, *Chem. Phys. Lett.* 108 (1984) 618–622.

[24] J.M. Herrmann, *New J. Chem.* 36 (2012) 883–890.

[25] H. Li, J. Li, Y. Huo, *J. Phys. Chem. B* 110 (2006) 1559–1565.

[26] H. Liu, Z. Lu, L. Yue, J. Liu, Z. Gan, C. Shu, T. Zhang, J. Shi, R. Xiong, *Appl. Surf. Sci.* 257 (2011) 9355–9361.

[27] H. Hao, J. Zhang, *Microporous Mesoporous Mater.* 121 (2009) 52–57.

[28] A. Kubacka, G. Colón, M. Fernández-García, *Appl. Catal. B* 95 (2010) 238–244.

[29] Q. Li, R. Xie, E.A. Mintz, J.K. Shang, *J. Am. Ceram. Soc.* 90 (2007) 3863–3868.

[30] A. Kubacka, B. Bachiller-Baena, G. Colón, M. Fernández-García, *Appl. Catal. B* 93 (2010) 274–281.

[31] M.S. Hybertsen, S.G. Louie, *Phys. Rev. B* 34 (1986) 5390–5413.

[32] R. Asahi, Y. Taga, *Phys. Rev. B* 61 (2000) 7459–7465.

[33] P. Wang, Z. Liu, F. Lin, G. Zhou, J. Wu, W. Duan, B.L. Gu, S.B. Zhang, *Phys. Rev. B* 82 (2010) 193103.

[34] W. Körner, C. Elsässer, *Phys. Rev. B* 83 (2011) 205135.

[35] Y. Gai, J. Li, S.S. Li, J.B. Xia, S.H. Wei, *Phys. Rev. Lett.* 102 (2009) 036402.

[36] T. Cottineau, N. Béalu, P.-A. Gross, S.N. Pronkin, N. Keller, E.R. Savinova, V. Keller, *J. Mater. Chem. A* 1 (2013) 2151–2160.

[37] Y. Liu, J.M. Szeifert, J.M. Feckl, B. Mandlmeier, J. Rathousky, O. Hayden, D. Fattakhova-Rohlfing, T. Bein, *ACS Nano* 4 (2010) 5373–5381.

[38] M. Hirano, K. Matsushima, *J. Am. Ceram. Soc.* 89 (2006) 110–117.

[39] S.H. Jang, H.C. Choe, Y.M. Ko, W.A. Brantley, *Thin Solid Films* 517 (2009) 5038–5043.

[40] Y. Furubayashi, T. Hitosugi, Y. Yamamoto, K. Inaba, G. Kinoda, Y. Hirose, T. Shimada, T. Hasegawa, *Appl. Phys. Lett.* 86 (2005) 252101.

[41] A. Ghicov, S. Aldabergenova, H. Tsuchiya, P. Schmuki, *Angew. Chem. Int. Ed.* 45 (2006) 6993–6996.

[42] Z. Xu, Q. Li, S. Gao, J.K. Shang, *J. Mater. Sci. Technol.* 28 (2012) 865–870.

[43] R.D. Shannon, *Acta Cryst.* 32 (1976) 751–767.

[44] A. Mattsson, M. Leideborg, K. Larsson, G. Westin, L. Österlund, *J. Phys. Chem. B* 110 (2006) 1210–1220.

[45] L. Yang, Y. Xiao, S. Liu, Y. Li, Q. Cai, S. Luo, *Appl. Catal. B* 94 (2010) 142–149.

[46] T. Mishra, M. Mahato, N. Aman, J.N. Patel, R.K. Sahu, *Catal. Sci. Technol.* 1 (2011) 609–615.

[47] C. Li, Z. Jiang, Z. Yao, *Dalton Trans.* 39 (2010) 10692–10696.

[48] B. Subramanian, R. Ananthakumar, M. Jayachandran, *Cryst. Res. Technol.* 46 (2011) 1273–1282.

[49] G. Jouve, C. Severac, S. Cantacuzene, *Thin Solid Films* 287 (1996) 146–153.

[50] A. Ghicov, M.J. Macak, H. Tsuchiya, J. Kunze, V. Heublein, S. Kleber, P. Schmuki, *Chem. Phys. Lett.* 419 (2006) 426–429.

[51] H. Cui, K. Dwight, S. Soled, A. Wold, *J. Solid State Chem.* 115 (1995) 187–191.

[52] K.S. Raja, M. Misra, V.K. Mahajan, T. Gandhi, P. Pillai, S.K. Mohapatra, *J. Power Sources* 161 (2006) 1450–1457.

[53] Z. Zhang, X. Wang, J. Long, Q. Gu, Z. Ding, X. Fu, *J. Catal.* 276 (2010) 201–214.

[54] X. Chen, C. Burda, *J. Phys. Chem. B* 108 (2004) 15446–15449.

[55] D. Joskowska, K. Pomoni, A. Vomvas, B. Koscielska, D.L. Anastassopoulos, *J. Non-Cryst. Solids* 356 (2010) 2042–2048.

[56] J. Tauc, R. Grigorovici, A. Vancu, *Phys. Status Solidi* 15 (1966) 627–637.

[57] G. Dai, J. Yu, G. Liu, *J. Phys. Chem. C* 115 (2011) 7339–7346.

[58] H. Liu, G. Liu, X. Shi, *Colloids Surf. A* 363 (2010) 35–40.

[59] Q. Li, M.A. Page, B.J. Marinās, J.K. Shang, *Environ. Sci. Technol.* 42 (2008) 6148–6153.

[60] Q. Li, Y.W. Li, P. Wu, R. Xie, J.K. Shang, *Adv. Mater.* 20 (2008) 3717–3723.

[61] Q. Li, Y.W. Li, Z. Liu, R. Xie, J.K. Shang, *J. Mater. Chem.* 20 (2010) 1068–1072.